Casimir force measurements from silicon carbide surfaces

M. Sedighi,[1] V. B. Svetovoy,[2,3] and G. Palasantzas[1]

[1]*Zernike Institute for Advanced Materials, University of Groningen, Nijenborgh 4, 9747 AG Groningen, The Netherlands*

[2]*MESA+ Institute for Nanotechnology, University of Twente, P. O. 217, 7500 AE Enschede, The Netherlands*

[3]*Institute of Physics and Technology, Yaroslavl Branch, 150007, Universitetskaya 21, Yaroslavl, Russia*

(Received 19 October 2015; revised manuscript received 23 January 2016; published 22 February 2016)

Using an atomic force microscope we performed measurements of the Casimir force between a gold- coated (Au) microsphere and doped silicon carbide (SiC) samples. The last of these is a promising material for devices operating under severe environments. The roughness of the interacting surfaces was measured to obtain information for the minimum separation distance upon contact. Ellipsometry data for both systems were used to extract optical properties needed for the calculation of the Casimir force via the Lifshitz theory and for comparison to the experiment. Special attention is devoted to the separation of the electrostatic contribution to the measured total force. Our measurements demonstrate large contact potential V_0 ($\approx$0.67 V), and a relatively small density of charges trapped in SiC. Knowledge of both Casimir and electrostatic forces between interacting materials is not only important from the fundamental point of view, but also for device applications involving actuating components at separations of less than 200 nm where surface forces play dominant role.

DOI: 10.1103/PhysRevB.93.085434

I. INTRODUCTION

Modern microelectromechanical and nanoelectromecanical systems (MEMS/NEMS) are becoming increasingly important in science and technology, which simultaneously reveal the significant role of the Casimir force for the analysis and design of microsytems or nanosystems [1]. This force between two objects arises due to the existence of quantum fluctuations of the electromagnetic (EM) field [1–12], as it was predicted by Casimir in 1948 [2] assuming two perfectly conducting parallel plates. Lifshitz and coworkers in the 1950's [3] considered the general case of real dielectric plates by exploiting the fluctuation-dissipation theorem, which relates the dissipative properties of the plates (via optical absorption by many microscopic dipoles) and the resulting EM fluctuations. The theory described correctly the attractive interaction due to quantum fluctuations for all separations covering both the Casimir (long-range or typically $>$ 20 nm) and van der Waals (short-range or typically $<$ 10 nm) regimes [1,3]. While the relation between the EM vacuum fluctuations and the Casimir force has some fundamental significance, the dependence of the Casimir force on material optical properties is an important aspect since, in principle, one can tailor the force by suitable choice of materials [5–15].

Up to now there have been a significant variety of materials used [5–16] for calculations and measurements of the Casimir force. It was confirmed that metals were the materials (e.g., Au is the one studied the most) that give the maximum Casimir force due to the high absorption of conduction electrons in low frequency ranges (far-infrared). Although most of the research was focused on the same interacting materials, the Casimir force between dissimilar metals has also been investigated [6–10,13–15]. However, metals are not always suitable for device applications if attributes such as high durability combined with high stiffness and low thermal expansion are necessary. On the other hand, a material that offers these special attributes is silicon carbide (SiC) [13–15], and it is currently utilized for precise instrumentation frames and mirrors, as well as there is a possibility to be used in macroassembly or nanoassembly technologies via direct (optical) bonding [17]. Moreover, for MEMS applications in the automotive industry and space applications [18,19], MEMS sensors are required to operate in harsh environments, which can be a challenge for Si sensing devices, while SiC is considered a substitute for Si due to its excellent properties. Indeed, the relatively low residual stress level in the layers, the high stiffness, and excellent etch-stop properties allow the fabrication of free-standing SiC microstructures using standard Si bulk micromachining techniques [18,19]. In addition, since SiC exhibits high hardness, chemical inertness, the ability to survive operation at high temperatures, as well as harsh corrosive environments [20,21], it is well suited as a protective coating of micromachined parts.

So far, however, there is limited knowledge about Casimir forces arising by interactions with SiC, besides theory predictions using measured optical data of SiC [22]. The measurement of the Casimir force for SiC as for any other dielectric material is complicated by trapping of electrical charges. This problem can be significantly reduced by doping of the material to make it slightly conductive [22]. Hence we performed here a comprehensive study to measure the Casimir force from conductive SiC surfaces using the sphere plate geometry in an atomic force microscope (AFM) with the sphere being gold-coated (Au). Significant focus was given to the involved electrostatics to determine the associated contact potentials between the sphere-plate, and possible remnant electrostatic forces due to uncompensated charges that can obscure the genuine Casimir interaction. At some point we would have to deal with this force when dimensions are reduced and more and more devices are loaded on a chip with components actuating at separations less than 200 nm. Therefore for the design and stability of MEMS, measuring the Casimir force is very essential knowledge since it provides unique opportunities for the analysis of device actuation under more realistic conditions.

II. EXPERIMENTAL PROCEDURE

Nitrogen-doped (N) SiC samples (thickness 400 μm and chemical-mechanical-polished) were obtained from university

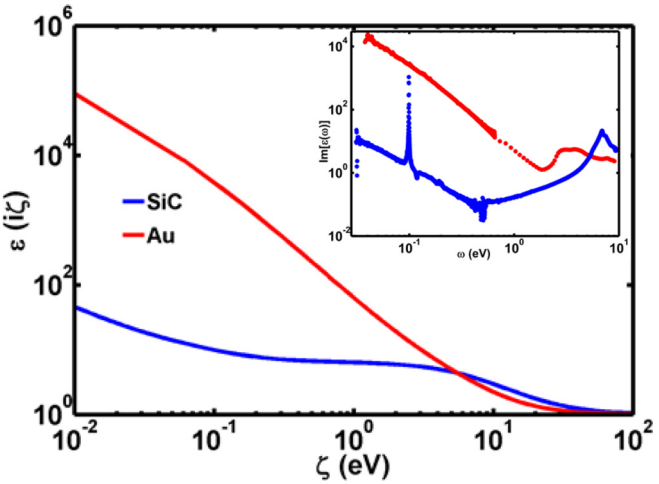

FIG. 1. Dielectric function of SiC and Au at imaginary frequencies, which it is used as input for Casimir force calculations via the Lifshitz theory. The inset shows the imaginary part $\varepsilon''(\omega)$ of the dielectric response functions as obtained by ellipsometry [22].

wafers (http://www.universitywafer.com/). Then the optical properties of the SiC samples were commercially characterized in J.A. Woollam Co., Inc. (http://www.jawoollam.com) with ellipsometry using the VUV-VASE (wavelengths 140 nm –2.5 μm) and IR-VASE (wavelengths 2 μm –30 μm) ellipsometers at three incident angles with respect to the sample surface $j = 55°,65°,75°$ [22]. Consequently, analysis of the data yielded the frequency-dependent dielectric function $\varepsilon(\omega)$, [22] and subsequently, the corresponding dielectric function at imaginary frequencies, see Fig. 1, which is necessary for Casimir force calculations.

Furthermore, for the measurement of the Casimir force we used a Bruker Pico Force AFM (operated in a dry N_2 atmosphere) in the sphere-plate geometry (see supplemental material Figs. A1 and A2 [23]), where a 20-μm in diameter sphere (Duke Scientific Borosilicate sphere) was glued on an Au-coated tipless cantilever [Fig. 2(a)]. This last had relatively high spring constant $k = 1.93$ N/m to minimize jump-to-contact due to the formation of a capillary meniscus at very close surface separations (<8 nm), which is also limited by the weak surface roughness of both the sphere and the plate surface [Figs. 2(b) and 2(c), see supplemental material Fig. A3 [23]). The Borosilicate sphere attached to the cantilever was coated with a 100-nm Au film, which was optically bulk, as well as ensuring electrical contact with the cantilever, therefore, allowing electrostatic calibration of the system by application of external potentials [24]. During electrostatic calibration, 15 force measurements were averaged for each applied potential V, and 40 000 data points were used for the various piezoramp sizes (∼3-7 μm). Finally, a low piezoapproach or piezoretraction speed of 50 nm/s was used to minimize any contribution from the repulsive hydrodynamic drag forces.

The topography of both the SiC plate and the sphere, which was used for the force measurements, was measured by AFM [including scanning electron microscopy (SEM) inspection] after complete preparation and prior to force measurements [Figs. 2(b) and 2(c)]. The roughness analysis

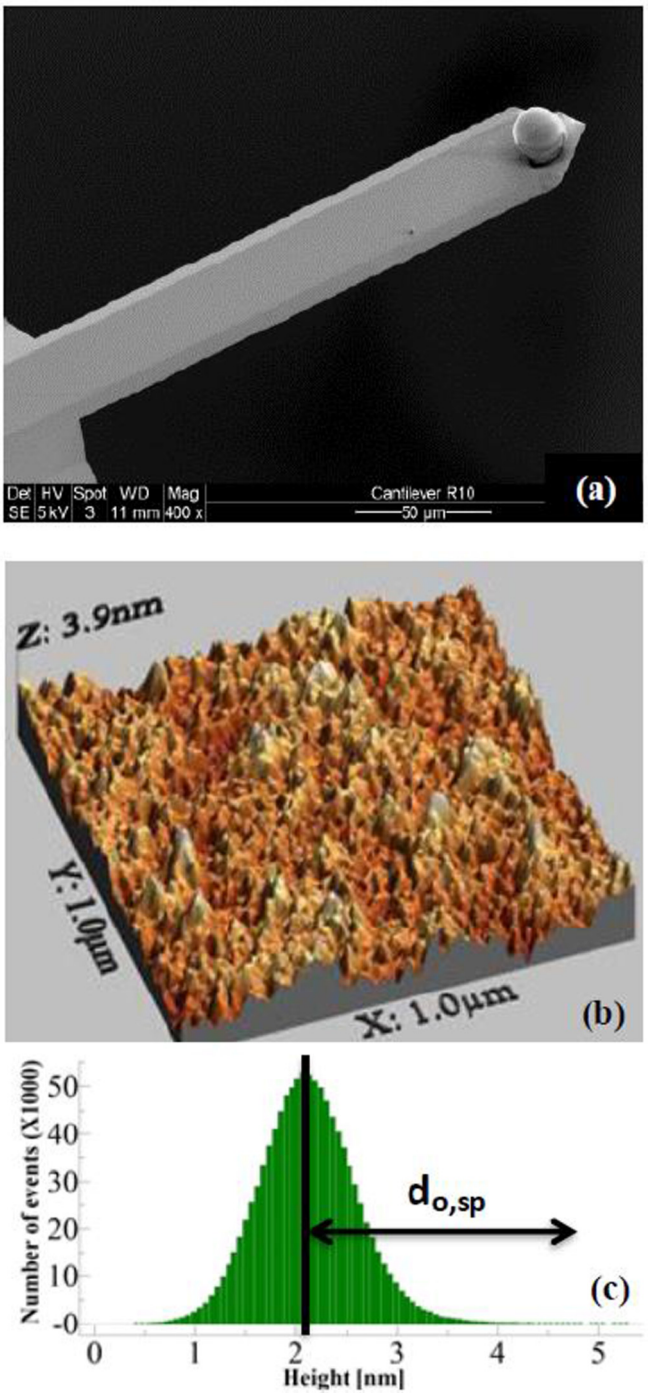

FIG. 2. (a) Top view scanning electron microscopy (SEM) image of a sphere attached on a cantilever. (b) AFM topography of the sphere after Au deposition obtained by scanning on top of the sphere. (c) Height distribution of the sphere roughness, which provides the dominant contribution $d_{o,sp}$ to distance upon conduct (for the SiC-Au system) due to the sphere roughness. Comparison shows that $d_{o,sp} \gg d_{o,SiC}$.

indicated almost atomically flat SiC surfaces with a root-mean-square (rms) surface roughness $w_{SiC} \approx 0.12$ nm, making the roughness contributions also to optical data analysis (Fig. 1) negligible [22]. In fact, the maximum surface peak of the SiC surface is at most $d_{o,SiC} \approx 0.8$ nm, as obtained by the

height histograms [25]. The AFM measurement of the sphere roughness after Au coating gave also a height distribution with a maximum surface peak at most $d_{o,Sph} \approx 2.5$ nm (see Fig. 2). Therefore, the maximum total distance upon contact of the sphere on the SiC surface limited due to random surface roughness (of both interacting surfaces) is estimated to be $d_{o,max} \approx d_{o,SiC} + d_{o,Sph} \approx 3.3$ nm if the highest peak at the SiC surface and the sphere surface are at the same location [25]. The latter is rarely true and for an average estimate for the total d_o (so that $d_o < d_{o,max}$) we consider $d_o \approx w_{SiC} + d_{o,Sph} \approx 2.6$ nm. These low roughness values allow the approach of the sphere on the plate at a separation less than 10 nm, which is limited only by jump-to-contact.

In fact, it is rather formidable to perform force measurements at surface separations less than 10 nm since spontaneous vapor condensation and the formation of the capillary meniscus (both interacting surfaces are hydrophilic) will lead to jump-to-contact even at separations $>d_o$ Spontaneous vapor condensation occurs on the average when the surface separation is comparable to $\approx 2R_k$, where R_k is given by the Kelvin equation $R_K = -(\gamma V_m/RT)[\log(RH)]^{-1}$ with γ being the liquid surface tension, RH is the relative humidity, and V_m is the molar liquid volume [26]. For water at $T = 300$ K and $\gamma = 73\,\mathrm{mJ/m^2}$ ($\gamma V_m/RT = 0.54$ nm [26]) we obtain $2R_K \sim 0.5 - 2.7$ nm with RH $\sim$ 1–40%. Therefore, the minimum possible separation prior to jump-to-contact is estimated to be $d_{min} \approx d_o + 2R_k$. Substitution yields $d_{min} \approx 3.1 - 5.3$ nm, which is comparable to our observations of jump-to-contact that took place at separations below 8 nm. As a result, attempts to perform force measurements in ambient were not successful because the capillary force due to meniscus formation was large (as it is expected for the weak surface roughness here [27]), and prevented cantilever retraction despite the use of several microns ramp sizes. This problem was alleviated by pumping the system down to $\sim 10^{-5}$ mbar and venting several times it with dry N_2 to reduce the capillary forces upon contact. Under these conditions the cantilever stiffness was proved too sufficient to overcome the capillary adhesion, and thus to perform force measurements despite the jump-to-contact at separations less than 10 nm. Note that at these high vacuum pressures one cannot fully eliminate water surface layers present on hydrophilic surfaces and the resulting capillary forces [27].

To translate the cantilever deflection graphs (with a deflection sensitivity of $\approx 53 \pm 5$ nm/V, see supplemental material Figs. B1 and B2 [23]) to force one has to know the cantilever spring constant. One method to obtain the spring constant is thermal tuning, which involves measuring the mechanical response of the cantilever due to agitations of impinging molecules from the surrounding fluid (e.g., air, gases, and liquids) and due to thermal dissipation via internal degrees of freedom. Within the N_2 environment thermal tuning from an average of 40 measurements gives the spring constant value $k = 2.01 \pm 0.2\,\mathrm{N/m}$. If we fit the electrostatic force curves at various large separations ($z > 500$ nm), it will yield a large spring constant $k = 2.3$–$2.8\,\mathrm{N/m}$. Disagreement with the thermal tuning demonstrates that application of Eq. (1) to SiC is not fully justified. This is because SiC is a poor conductor with a finite Debye length and small but measurable concentration of charges trapped on the surface (see below). Precise force measurements require more accurate estimation of the spring constant, which is not satisfied either using thermal tuning with accuracy in general $\sim 10\%$ [28] or applying Eq. (1) which is applicable for a metallic conductor. Therefore, we used an Au-coated plate (made also during deposition of Au onto the sphere) for calibration [24] instead of the SiC plate, and the spring constants were obtained with 3% accuracy to be $K = 1.93 \pm 0.06\,\mathrm{N/m}$ (see supplemental material Fig. B3 [23]). Note that this value is in agreement with k determined from the thermal tuning.

III. ELECTROSTATIC AND CASIMIR FORCE MEASUREMENTS

Electrostatic calibration was performed by applying various potentials and measuring the cantilever deflection versus sphere-plate separation (see supplemental material Figs. B1 and B2 [23]). From these data we can obtain the experimental Casimir force and the contact potential which is not varying with separation distance. For metallic conductive (e.g., metals) surfaces, the electrostatic force in the sphere-plate geometry for an applied voltage V is given by [24]

$$F_{el} = X(z)(V - V_0)^2\,,$$
$$X(z) = 2\pi\epsilon_0 \sum_{n=1}^{\infty} [csc^{-1}(n\alpha)(\coth\alpha - n\coth n\alpha)] \quad (1)$$

with $\alpha = \cosh^{-1}[1 + (z + d_0)/R]$, z the sphere-plate separation distance, d_o is the distance upon contact due to the roughness of both the sphere and plate, ε_o the intervening medium dielectric constant, R the sphere radius, and V_o the contact potential between sphere and the plate (e.g., due to different work functions of the interacting materials). The voltage dependence $F_{el} \sim (V - V_o)^2$ indicates that the electrostatic force is minimized for $V = V_o$ allowing the determination of the contact potential V_o from the position of the minimum in a F_{el} versus V curve (see Fig. 3). Prior to any data analysis the nonlinear signal contributions (though in various cases can be treated as a linear signal), due to backscattered light by the plate surface into the photodiode of the AFM, was subtracted from all the deflection measurements. This is performed by fitting the large separation range (>600 nm) using a second degree polynomial (see supplemental material Fig. B2, after data average from 30 experiments [23]) for $V = 0$. Figure 3(a) shows the cantilever deflection versus applied voltage V (for $-4 < V < 4$ Volts) for the same sphere-plate separation. The parabolic behavior of the deflection data, in relative good agreement with Eq. (1), indicates that the minimum corresponds to an effective contact potential $V = V_o$. Plotting V_o versus separation z in Fig. 3(b) also shows a slight variation of V_o in the range ~ 0.67–0.68 V for separations 0.5–2 μm. In addition, Kelvin probe force microscopy (KPFM) [29] has been used to study the local variation of the contact potential of the SiC surface (see supplemental material Fig. B4 [23]). The potential revealed a peak-to-peak variation ~ 0.67 V, which is comparable in magnitude with V_o obtained from electrostatic measurements. The large variation of the SiC potential can indicate significant contribution of patch potentials to the total force, explaining the origin of the deviations between theory

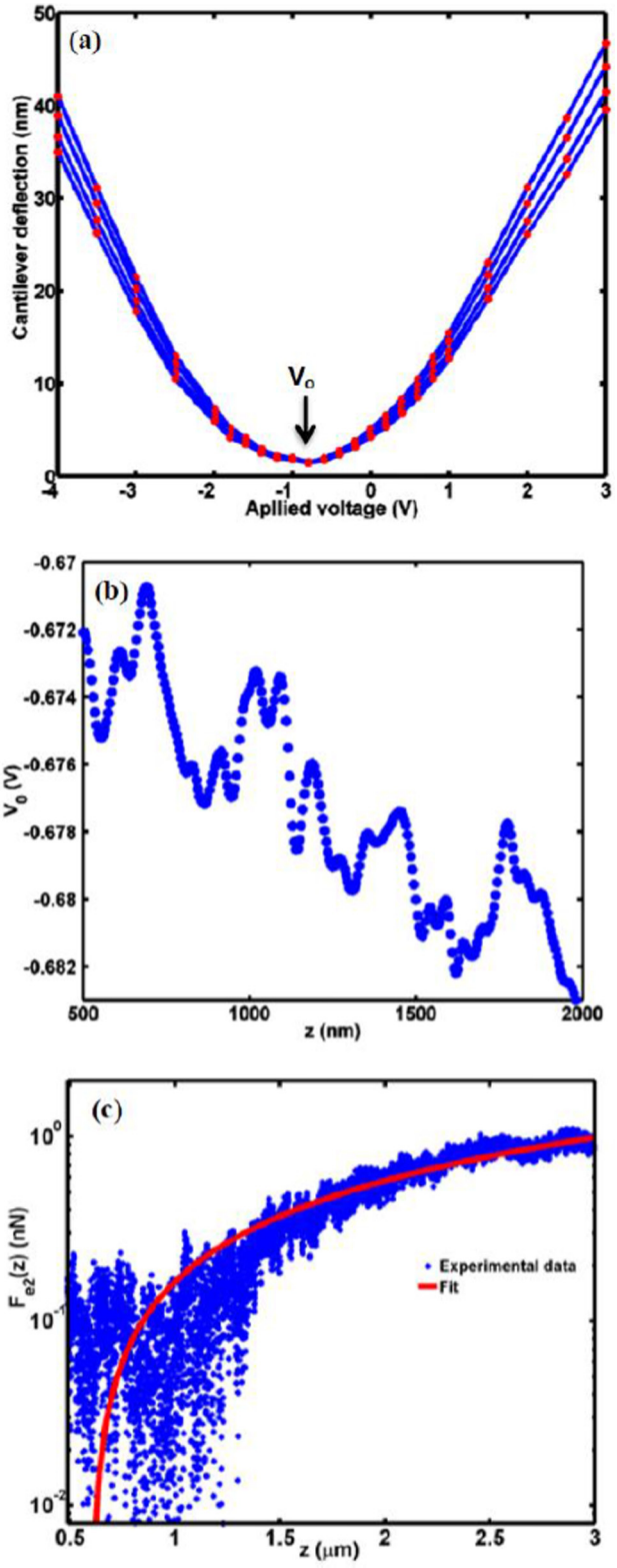

FIG. 3. (a) Cantilever deflection versus applied voltage $-4 < V < 3$ with the voltage at the minimum providing the contact potential V_o. The different deflection for the same potential corresponds to different sphere-plate separation. (b) Variation of V_o vs. separation. (c) Remnant cantilever deflection (with potential compensation $V = V_o$) due to uncompensated charges on the SiC plate. Fitting with the logarithmic form $F_{e2}(z) = k[c_1 \log(z) + c_2]$ yields the parameter values $c_1 = 0.52$ nm and $c_2 = 0.27$ nm.

and experiment as we will see in the following at short ranges (<50 nm).

Nonetheless, as Fig. 3(a) indicates, the minimum deflection at $V = V_o$ is not zero, and consequently an uncompensated remnant electrostatic contribution is still present. By considering several data points with varying applied potential, we fitted the deflection data versus V, e.g., as in Fig. 3(a), with the form $\Delta_t = (X(z)/k)(V - V_0)^2 + A(z)$, where Δ_t represents the total deflection and the parameter $A(z)$ is an additional deflection at $V = V_o$ due to the net charge trapped on the SiC surface. These charges have high binding energy and are essentially immobilized. They are similar to charge collected on a dielectric surface but the density is much smaller. When the contact potential is compensated ($V = V_o$) these charges are still active. It is not simple to describe the effect of remnant charges theoretically because their contribution diverges for infinite plate dimensions and proximity force approximation (PFA) cannot be applied. Due to the divergence one has to solve the electrostatic problem in the volume that is comparable in size with the SiC plate. For this reason all the specific geometry of the experiment will be important. On the other hand, we can determine the force due to uncompensated charges experimentally. Figure 3(c) shows that the remnant deflection $A(z)$, and consequently the remnant electrostatic force $F_{e2} = kA(z)$. Assuming the weakest logarithmic divergence with the distance one would expect the following dependence $A(z) = c_1 \log(z) + c_2$, where c_1 is related to the density of surface charges and the parameter c_2 depends on the bodies surrounding the SiC plate. The parameters $c_{1,2}$ were obtained by fitting the deflection data at separations $z \sim$1-3 μm. From Fig. 3(c) one can see that the agreement with the deflection data is very good. An estimation gives a variation for the remnant force $F_{e2} \sim 0.09 - 0.95$ nN for $z \sim$1-3 μm [Fig. 3(c)]. This uncompensated force, with respect to the Casimir force, will be more significant at larger surface separations (>1 μm), while for our actuation studies it will remain small below 300 nm.

Nonetheless, the high contact potential V_o implies that an electrostatic compensation will be necessary for device actuation, if the contribution of the Casimir force is to play the role of the dominant actuating force at shorter separations (≤300 nm). Force measurements performed with a compensating potential $V = V_o$ to remove the main electrostatic contribution, $\sim (V - V_o)^2$, are shown in Fig. 4. Note that to translate the cantilever deflection to the force we used the spring constant $k = 1.93$ N/m determined, as explained above, using electrostatic calibration but for an Au-coated plate. Finally, to understand at what ranges we can use Lifshitz theory [3,11,25,30] to compute the Casimir force for systems involving SiC, we compare in Fig. 4 the force measurements to predictions of the Lifshitz theory using as input the measured optical data for SiC and Au (Fig. 1) [22].

Analysis of the optical data has shown a significant concentration of charge carriers, which give a small Debye screening length $1_D \approx 1$ nm at $T = 300$ K so that one can neglect the effects of poor conductivity resulting in nonlocal response of the material for separations $z > l_D$[22]. In addition, thermal effects at the separations $z \lesssim 300$ nm, where we explore actuation dynamics, can be neglected. Therefore we utilized for Casimir force calculations the convenient representation

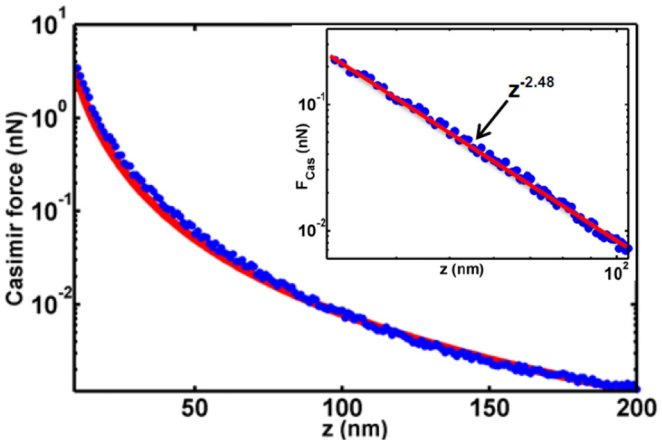

FIG. 4. Experimental force measurements at compensating potential $V = V_o$, and comparison to the Lifshitz theory calculations of the Casimir force in the range between 10-200 nm (using as input for SiC the optical data from Fig. 1, and for Au measured data from [11]). The inset shows a log-log fit to obtain the scaling exponent for Casimir force $F_{\rm Cas} \sim z^{-\rm m}$.

at $T = 0\,\rm K$ (using the PFA for the sphere-plate geometry and assuming $z \ll \rm R$ [3,11,25,30]),

$$F_{\rm Cas}(z) = \frac{\hbar c R}{16\pi z^3} \sum_{\nu} \int_0^1 dt \int_0^\infty dx x^2 \ln\left(1 - r_1^\nu r_2^\nu e^{-\rm x}\right). \quad (2)$$

The integration variables are defined as $x = 2k_0 z, t x = \zeta/\zeta_{\rm ch}$ and $\zeta_{\rm ch} = c/2z$. $\rm k_0 = \sqrt{(\zeta^2/c^2) + q^2}$ and $\rm k_i = \sqrt{\varepsilon_i(i\zeta)(\zeta^2/c^2) + q^2}$ are, respectively, the wave numbers perpendicular to the plate in air and in the each material, as well as q is the wave number along the plate. The index $\nu =$ s (TE mode)andp (TM mode) denotes the two polarizations, and $\rm r^\nu_{1,2}$ the corresponding Fresnel reflections coefficients. The latter are defined as

$$\begin{aligned} \rm r_i^s &= \frac{1 - \sqrt{1 + t^2(\varepsilon_i(i\zeta) - 1)}}{1 + \sqrt{1 + t^2(\varepsilon_i(i\zeta) - 1)}}, \\ \rm r_i^p &= \frac{\varepsilon_i - \sqrt{1 + t^2(\varepsilon_i(i\zeta) - 1)}}{\varepsilon_i + \sqrt{1 + t^2(\varepsilon_i(i\zeta) - 1)}}. \end{aligned} \quad (3)$$

As Fig. 4 shows, the measured force has a good agreement with the Lifshitz theory prediction in range above 60 nm, which, however, at short ranges ($z < 30$ nm) neglects the influence of surface roughness [25]. The log-log plot of the force indicates an average power law dependence in the range $z \sim$10–100 nm $F_{\rm Cas}(z) \sim z^{-2.48}$, which is in agreement with findings from other interacting systems where $F_{\rm Cas} \sim z^{-\rm m}$ and $m < 3$ for the sphere-plate geometry [12,31]. Using this information the relative error in the force due to uncertainty in the spring constant and in the surface separations is estimated as $\Delta F_{\rm Cas}/F_{\rm Cas} \approx [(\Delta k/k)^2 + (2.48\Delta z/z)^2]^{1/2}$. If we consider $\Delta k/k \approx 0.1$ from the thermal tuning, and $\Delta z \approx 1$ nm due to surface roughness [25] at the point close to contact $z \approx 8\,\rm nm$ (where jump-to-contact occurs), the maximum relative error is $\Delta F_{\rm Cas}/F_{\rm Cas} \approx 31\%$ at $z = 8\,\rm nm$, and $\Delta F_{\rm Cas}/F_{\rm Cas} \approx 5\%$ at $z = 100\,\rm nm$ (limited by the error in the spring constant $\Delta k/k$). Within the error estimations, taking into account the error between force measurement and the Lifshitz theory (see supplemental material Fig. C1 [23]), the agreement between the Lifshitz theory and measurements at separations below 200 nm, where several actuation studies have taken place [13–15,22,32], is well justified.

IV. CONCLUSION

In conclusion, we performed measurements of the Casimir force between a gold-coated (Au) sphere and conductive silicon carbide (SiC) samples, which are promising materials for devices operating in severe environments. For this purpose the roughness of SiC and Au surfaces were also measured with the AFM to obtain information of the minimum distance upon contact, as well as the optical properties of the interacting surfaces were characterized with ellipsometry to allow the calculation of the Casimir force via the Lifshitz theory and compare to the experimental force results. Attention was given to the separation of the electrostatic contribution from the measured total force. Our measurements demonstrated large contact potential $\rm V_0$ (≈0.67 V), and a relatively small density of charges trapped in SiC. Knowledge of both Casimir and electrostatic forces between interacting materials is important for applications involving actuating components of devices at short separations (<200 nm) where surface forces play a dominant role.

ACKNOWLEDGMENT

We would like to acknowledge support from the Zernike Institute of Advanced Materials, University of Groningen, The Netherlands.

[1] A. W. Rodriguez, F. Capasso, and S. G. Johnson, Nat. Photon. **5**, 211 (2011); P. Ball, Nature (London) **447**, 772 (2007).
[2] H. B. G. Casimir, Proc. K. Ned. Akad. Wet. **51**, 793 (1948).
[3] E. M. Lifshitz, Sov. Phys. JETP **2**, 73 (1956); I. E. Dzyaloshinskii, E. M. Lifshitz, and L. P. Pitaevskii, Sov. Phys. Usp. **4**, 153 (1961).
[4] S. K. Lamoreaux, Phys. Rev. Lett **78**, 5 (1997); Rep. Prog. Phys. **68**, 201 (2005); H. B. Chan, V. A. Aksyuk, R. N. Kleiman, D. J. Bishop, and F. Capasso, Phys. Rev. Lett. **87**, 211801 (2001); H. B. Chan *et al.*, Science **291**, 1941 (2001); R. S. Decca *et al.*, Ann. Phys. (NY) **318**, 37 (2005); R. S. Decca, D. Lopez, E. Fischbach, G. L. Klimchitskaya, D. E. Krause, and V. M. Mostepanenko, Phys. Rev. D **75**, 077101 (2007).
[5] D. Iannuzzi, M. Lisanti, and F. CapassoProc. Natl. Acad. Sci. USA **101**, 4019 (2004).
[6] F. Chen, G. L. Klimchitskaya, V. M. Mostepanenko, and U. Mohideen, Optics Express **15**4823 (2007); G. Torricelli, I. Pirozhenko, S. Thornton, A. Lambrecht, and C. Binns, Europhys. Lett. **93**, 51001 (2011).

[7] S. de Man, K. Heeck, R. J. Wijngaarden, and D. Iannuzzi, Phys. Rev. Lett. **103**, 040402 (2009).
[8] G. Torricelli, P. J. van Zwol, O. Shpak, C. Binns, G. Palasantzas, B. J. Kooi, V. B. Svetovoy, and M. Wuttig, Phys. Rev. A **82**, 010101 (R) (2010).
[9] G. Torricelli, P. J. van Zwol, O. Shpak, G. Palasantzas, V. B. Svetovoy, C. Binns, B. J. Kooi, P. Jost and M. Wuttig, Advanced Functional Materials **22**, 3729 (2012).
[10] C.-C. Chang, A. A. Banishev, G. L. Klimchitskaya, V. M. Mostepanenko, and U. Mohideen, Phys. Rev. Let. **107**, 090403 (2011).
[11] V. B. Svetovoy, P. J. van Zwol, G. Palasantzas, and J. Th. M. DeHosson, Phys. Rev. B. **77**, 035439 (2008).
[12] G. Palasantzas, V. B. Svetovoy, and P. J. van Zwol, International Journal of Modern Physics B **24**, 6013 (2010).
[13] M. Sedighi, W. H. Broer, G. Palasantzas, and B. J. Kooi, Phys. Rev. B **88**, 165423 (2013).
[14] M. Sedighi, W. H. Broer, S. Van der Veeke, and V. B. Svetovoy and G Palasantzas, J. Phys: Cond. Matt. **27**, 214014 (2015).
[15] M. Sedighi and G. Palasantzas, J. Appl. Phys. **117**, 144901 (2015).
[16] R. S. Decca, D. Lo´pez, E. Fischbach, and D. E. Krause, Phys. Rev. Lett. **91**, 050402 (2003).
[17] J. Haisma, N. Hattu, J. T. C. M. Pulles, E. Steding, and J. C. G. Vervest, Appl. Opt. **46**, 6793 (2007); J. Haisma and G. A. C. M. Spierings, Philips J. Res. **49**, 47 (1995); Jan Haisma and G. A. C. M. Spierings, Materials Science and Engineering: R: Reports 37 (1-2) 1-60 (202).
[18] R. Cheung, *Silicon Carbide MEMS for Harsh Enviroments*, edited by R. Cheung (University of Edinburgh, Edinburgh, Scotland, 2006), Chap. 1.
[19] B. Stark, *MEMS Reliability Assurance Guidelines for Space Applications*, Vol. 99 (Jet Propulsion Laboratory, Pasadena, CA), p. 1.
[20] MRS Bulletin, *Silicon Carbide Electronic Materials and Devices*, Vol. 22, No. 3, March 1997, pp. 19–56.
[21] P. M. Sarro, Sensors and Actuators A: Physical **82**, 210 (2000).
[22] M. Sedighi, V. B. Svetovoy, W. H. Broer, and G. Palasantzas, Phys. Rev. B **89**, 195440 (2014).
[23] See Supplemental Material at http://link.aps.org/supplemental/10.1103/PhysRevB.93.085434 for (i) force measurement setup, (ii) electrostatic calibration and KPFM measurements, and (iii) force calculations and measurements.
[24] B. W Harris, F. Chen, and U. Mohideen, Phys. Rev. A **62**, 052109 (2000); A. Roy, C. Y. Lin, and U. Mohideen, Phys. Rev. D **60**, 111101 (1999); U. Mohideen and A. Roy, Phys. Rev. Lett. **81**, 4549 (1998); H.-C. Chiu, C.-C. Chang, R. Castillo-Garza, F. Chen, and U. Mohideen, J. Phys. A: Math. Theor. **41**, 164022 (2008); W. R. Smythe, *Electrostatics and Electrodynamics* (McGraw-Hill, New York, 1950).
[25] P. J. van Zwol, V. B. Svetovoy, and G. Palasantzas, Phys. Rev. B **80**, 235401 (2009); W. Broer, G. Palasantzas, J. Knoester, and V. B. Svetovoy, *ibid.* **85**, 155410 (2012); W. H. Broer, G. Palasantzas, J. Knoester, and V. B. Svetovoy, Europhys. Lett. **95**, 30001 (2011).
[26] J. Israelachvili, *Intermolecular and Surface Forces*, 3rd ed. (Academic, New York, 1992); H.-J. Butt, B. Cappella, and M. Kappl, Surf. Sci. Rep. **59**, 1 (2005); R. Maboudian and R. T. Howe, J. Vac. Sci. Technol. B **15**, 1 (1997).
[27] P. J. van Zwol, G. Palasantzas, and J. Th. M. De Hosson, Phys. Rev. E **78**, 031606 (2008).
[28] B. Ohler, Rev. Sci. Inst. **78**, 063701 (2007).
[29] S. Sadewasser and T. Glatzel, *Kelvin Probe Force Microscopy: Measuring and Compensating Electrostatic Forces* (Springer, Heidelberg, Germany, 2011).
[30] C. D. Foscoa, Fernando C. Lombardoc, and F. D. Mazzitelli, Ann. Phys. (NY) **327**, 2050(2012).
[31] V. B. Svetovoy and G. Palasantzas, Adv. Colloid Interface Sci. **216**, 1 (2015).
[32] W. Broer, G. Palasantzas, J. Knoester, and V. B. Svetovoy, Phys. Rev. B **87**, 125413 (2013); R. Esquivel-Sirvent, L. Reyes, and J. Bárcenas, New J. Phys. **8**, 241 (2006); R. Esquivel-Sirvent, M. A. Palomino-Ovando, and G. H. Cocoletzi, Appl. Phys. Lett. **95**, 051909 (2009).